J. Fluid Mech. (2023), *vol*. 959, A19, doi:10.1017/jfm.2023.73

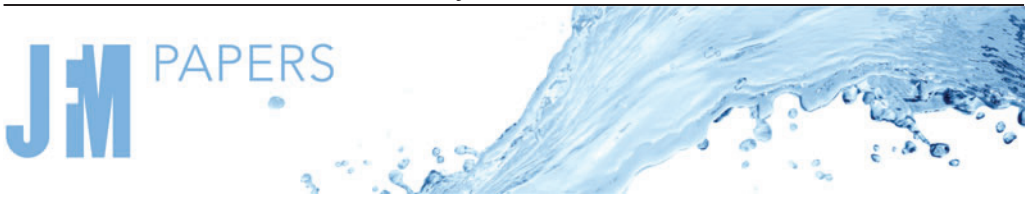

Freak wave in a two-dimensional directional wavefield with bottom topography change. Part 1. Normal incidence wave

Zuorui Lyu[1], **Nobuhito Mori**[2,3],† **and Hiroaki Kashima**[4]

[1]Coastal Engineering Laboratory, Department of Civil Engineering, School of Engineering, The University of Tokyo, Bunkyo-ku, Tokyo 113-8656, Japan

[2]Disaster Prevention Research Institute, Kyoto University, Gokasho, Uji, Kyoto 611-0011, Japan

[3]Swansea University, Bay Campus, Skewen, Swansea SA1 8EN, UK

[4]Coastal and Ocean Engineering Department, Port and Airport Research Institute, 3-1-1 Nagase, Yokosuka, Kanagawa 239-0826, Japan

(Received 25 June 2022; revised 17 December 2022; accepted 19 January 2023)

In the propagation and evolution of sea waves, previous studies pointed out that the occurrence of the freak wave height is significantly related to the quasi-resonant four-wave interaction in the modulated waves. From numerical–experimental study over an uneven bottom, the nonlinear effect caused by the bathymetry change also contributes to the occurrence of extreme events in unidirectional waves. To comprehensively analyse the two-dimensional wavefield, this study develops an evolution model for a directional random wavefield based on the depth-modified nonlinear Schrödinger equation, which considers the nonlinear resonant interactions and the wave shoaling the shallow water. Through Monte Carlo simulation, we discuss the directional effect on the four-wave interaction in the wave train and the maximum wave height distribution from deep to shallow water with a slow varying slope. The numerical result indicates that the directional spreading has a dispersion effect on the freak wave height. In a shallow-water environment, this effect becomes weak, and the bottom topography change is the main influencing factor in the wave evolution.

Key words: coastal engineering, nonlinear instability, shallow water flows

1. Introduction

With the development of the technology in observation and recording, the rogue/freak/extreme wave (from now on called a ‘freak wave’) has been generally recognized

† Email address for correspondence: mori@oceanwave.jp

as a kind of marine disaster instead of a small probability event in special circumstances. The concept of the freak wave was first suggested by Draper (1965), and it occurs when the wave height abnormally exceeds the significant wave height by a factor 2. Under different conditions, the occurrence probability of the freak wave clearly varies, which inspires us to think that the influence mechanism in wave height distribution is more complicated than generally expected.

Research to date indicates that the generation mechanism of the freak wave can be divided into internal and external factors. For the internal factors, the nonlinear interaction plays an important role in the occurrence of freak waves. Through a nonlinear wave evolution model, Benjamin (1967) indicated that modulational instability, a phenomenon leading to the energy concentration in a narrow-spectrum wave train, will make the waveform of surface gravity waves significantly unstable in deep water. After the 1990s, it was considered an important cause of freak waves behaving as four-wave interactions in the nonlinear wave model. In the study of Janssen (2003), the instability in Benjamin (1967) is actually an example of a non-resonant four-wave interaction in which the carrier wave is phase-locked with the sidebands. Based on the four-wave interactions and random wave statistics, a complete prediction model of freak waves in deep water is given by Janssen (2003) and Mori & Janssen (2006) and is verified by wave tank experiments (e.g. Mori *et al.* 2007; Kashima & Mori 2019). When it comes to the external factors, the bathymetry effect, the interaction with current, wind force and others contribute to the evolution of the nonlinear wave to varying degrees. The bathymetry effect on the water depth and local topography change have been known as significant influencing factors in the second-order nonlinear wave evolution.

For a more general explanation of freak wave occurrence, we need to consider the synthetic effect of internal and external factors. For a uniform unidirectional wave train, the modulational instability has a critical water depth at $kh = 1.363$ (k, wave number; h, water depth) from Benjamin (1967). When $kh < 1.363$, the modulational instability disappears, which implies the occurrence of a freak wave in relatively shallow water may decrease due to the attenuation of four-wave interactions. However, when it comes to a directional wavefield without limiting ourselves to collinear instabilities, there is no critical water depth such as $kh = 1.363$ due to the transversal disturbance (Benney & Roskes 1969; McLean *et al.* 1981). If we think that the four-wave interactions play an important role in the occurrence of the freak wave, the variation of water depth seems to be a non-negligible influencing factor. From the observation record, such as the World Ocean and the coast in Nikolkina & Didenkulova (2011), the freak wave occurs in deep water and finite and shallow water. Therefore, further investigation of the evolution of the four-wave interactions in the nonlinear modulated wave with the variation of bottom topography is necessary to study freak wave behaviours both offshore and onshore.

For a weakly dispersive long-wave train, its propagation process can be summarized by a partial differential equation in time and space. The nonlinear Schrödinger (NLS) equation (e.g. Zakharov 1968; Davey & Stewartson 1974), which can reflect the nonlinear effect caused by modulation interactions, is widely used to describe the amplitude evolution. From its standard format, a constant depth can be extended to a modified form with varying depth, considering spatial inhomogeneity. For example, Djordjević & Redekopp (1978) derived a solution for an envelope-hole soliton moving over an uneven bottom and gave a depth-modified NLS (dNLS) equation with a slope effect. Variation of the depth in Liu & Dingemans (1989) was divided into different scales, and then they gave evolution equations for modulated wave groups over an uneven bottom of different types. The evolution of a

modulated wave train over an uneven bottom is also discussed in Peregrine (1983), Turpin, Benmoussa & Mei (1983) and Mei & Benmoussa (1984).

Several numerical studies of the different nonlinear evolution equations have been given, such as the NLS-like equation (Zeng & Trulsen 2012; Kimmoun *et al.* 2021; Lyu, Mori & Kashima 2021), the Korteweg–De Vries (KdV) equation (Sergeeva, Pelinovsky & Talipova 2011; Majda, Moore & Qi 2019), Boussinesq equations (Gramstad *et al.* 2013; Kashima, Hirayama & Mori 2014; Zhang *et al.* 2019) and other nonlinear methods (Viotti & Dias 2014; Zheng *et al.* 2020; Lawrence, Trulsen & Gramstad 2021, etc.). From the research mentioned above, a similar conclusion can be derived, that is, the increase of bottom slope angle will give rise to inhomogeneity of the wavefield and lead to an increase of the kurtosis of surface elevation in very shallow water, which equals to the increase of the exceedance probability of extreme wave height $P_m(H_{max})$ occurring; here P_m represents the cumulative distribution function (CDF) and H represents wave height. The abrupt slope change, like the demarcation point between the sloping section (deep to shallow) and the flat bottom, gives a significant increase of $P_m(H_{max})$ as well as the skewness μ_3 of the surface elevation, which suggests the bathymetry effect is more reflected by the second-order effect. If we compare the numerical results in flat bottoms with different water depths, $P_m(H_{max})$ decreases from deep to medium water, as well as the kurtosis μ_4 of surface elevation, and it corresponds to Benjamin's (1967) result of the evolution of modulational instability: in shallow water $kh \leq 1.363$, modulational instability disappears and μ_4 shows an inverse effect on the unidirectional wave train in the deep-water case. The variation of $P_m(H_{max})$ with depth change can also be referred to Mendes *et al.* (2022), in which the second-order theory provides a physical explanation about wave statistics.

A similar process in shallow water can be verified in experiments. Physical modelling experiments can provide a reference for the steeper slope case and more variety of bottom topography as shown by Trulsen, Zeng & Gramstad (2012), Kashima *et al.* (2014), Ma, Dong & Ma (2014), Bolles, Speer & Moore (2019), Zhang *et al.* (2019), Kashima & Mori (2019), Trulsen *et al.* (2020) and Lawrence *et al.* (2021), Lawrence, Trulsen & Gramstad (2022). The values of kurtosis μ_4 and skewness μ_3 show a local maximum near the edge between the sloping bottom and flat bottom (deep to shallow). As the slope angle becomes very steep, this local maximum reaches its peak at the abrupt depth transitions in shallow water (Zheng *et al.* 2020; Li *et al.* 2021).

It should be pointed out that most of the numerical and experimental studies to date concentrate on the unidirectional wave train. The wave behaviours in the natural state are a two-dimensional (2-D) hydrodynamic problem. The stability of deep-water random waves in 2-D space is discussed in Alber & Saffman (1978). For long-crested irregular waves propagating over 2-D bathymetry, Lawrence *et al.* (2022) discussed the statistical properties of the surface elevation and the velocity field through numerical simulation using the high-order spectral method. In addition, a 2-D wavefield model can provide the directional wave spreading due to wind or current effect and the dispersion in one more horizontal dimension. Recent works show that the four-wave interaction decreases due to the directional dispersion effects. The maximum wave height in a directional wavefield decreases with the unidirectional wave in numerical simulation through a modified form of the NLS equation in Gramstad & Trulsen (2007). The enhancement of kurtosis is significantly suppressed by the increase of directional spread in the directional wave in Waseda (2006), Waseda, Kinoshita & Tamura (2009) and Onorato *et al.* (2009*a*,*b*). Based on the contribution from the directional bandwidth in the directional spectrum, Mori, Onorato & Janssen (2011) gave the theoretical estimation of kurtosis for directional sea

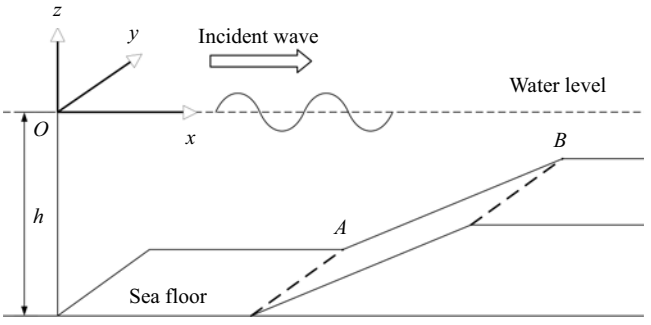

Figure 1. Sketch of the wave propagating over an uneven bottom in a 2-D wavefield.

states, and the fourth-order cumulant and directional spreading can predict the occurrence probability of freak waves. However, a comprehensive discussion about the bathymetry effect on the 2-D modulated wave is still to be had.

To develop the freak wave analysis in 2-D wavefields, this study investigates the directional nonlinear modulated wave evolution in an uneven bottom as an expansion to the work of Lyu *et al.* (2021). The dNLS equation in 2-D form for a slow-varying bottom is applied to establish the numerical model. In a 2-D wave basin, we consider the directional dispersion effect as part of the initial value problem and discuss how to compare the roles in the wave evolution of different parameters such as the slope angle, the water depth and directional spreading. Random wave statistics and a Monte Carlo simulation are conducted to give the evolution of the nonlinear effect and the distribution of extreme events in 2-D space–time (2-D + T). Section 2 gives the derivation of the theoretical model and its numerical solution. Section 3 gives the computation result and the discussion, and they are summarized in § 4. This article concentrates on the case when the wave is normally incident with the contour line of the bottom, so we do not consider the wave refraction. The oblique wave case will be given in the later work, Part 2.

2. Methodology

2.1. *Two-dimensional dNLS equation for an uneven bottom*

For a 2-D flow field, we continue to assume the flow is irrotational, inviscid and incompressible with a free water surface. A coordinate system (x, y, z) is defined with origin O, as shown in figure 1. Plane Oxy is defined along the quiescent water surface, and z axis is defined in the vertically upward direction, opposite to gravitational acceleration g. An incident directional random wave train comes from an external field, and its principal wave direction is along the x axis. The bottom $z = -h(x, y)$ mainly varies in the principal direction in the region between dashed lines A and B. Velocity potential Φ and free surface elevation η are defined as

$$\Phi = \Phi(x, y, z, t), \quad \eta = \eta(x, y, t), \tag{2.1}$$

where t represents time.

In the entire flow field, Φ is a solution of the Laplace equation to satisfy continuity

$$\nabla^2\Phi = \frac{\partial^2\Phi}{\partial x^2} + \frac{\partial^2\Phi}{\partial y^2} + \frac{\partial^2\Phi}{\partial z^2} = 0. \tag{2.2}$$

On the boundary of the free surface $z = \eta(x, y, t)$, Φ and η satisfy the kinematic boundary condition (i.e. free surface equation) and the dynamic boundary condition (i.e. Bernoulli equation)

$$\frac{\partial \Phi}{\partial z} = \frac{\partial \eta}{\partial t} + \frac{\partial \Phi}{\partial x}\frac{\partial \eta}{\partial x} + \frac{\partial \Phi}{\partial y}\frac{\partial \eta}{\partial y}, \quad z = \eta, \tag{2.3}$$

$$2\frac{\partial \Phi}{\partial t} + 2g\eta + \left(\frac{\partial \Phi}{\partial x}\right)^2 + \left(\frac{\partial \Phi}{\partial y}\right)^2 + \left(\frac{\partial \Phi}{\partial z}\right)^2 = 0, \quad z = \eta. \tag{2.4}$$

At the bottom of the flow field, Φ satisfies the no-flux boundary along the seafloor. If the water depth h is constant at a flat bottom $z = -h$, Φ satisfies the flat bottom equation

$$\frac{\partial \Phi}{\partial z} = 0, \quad z = -h. \tag{2.5}$$

If we assume, the bottom is uneven, and water depth varies at $z = -h(x, y)$, Φ satisfies the uneven bottom equation

$$\frac{\partial \Phi}{\partial z} + \frac{\partial h}{\partial x}\frac{\partial \Phi}{\partial x} + \frac{\partial h}{\partial y}\frac{\partial \Phi}{\partial y} = 0, \quad z = -h(x, y). \tag{2.6}$$

Based on the periodicity of time and space in the propagation of gravity waves, wave frequency ω and wavenumber k satisfy the linear dispersion relation

$$\omega = \sqrt{gk\sigma}, \tag{2.7}$$

where $\sigma = \tanh kh$. For a medium that has no temporal variation, carrier wave frequency $\omega = \omega_0$, where subscript 0 represents a constant angular frequency independent of the variable bathymetry. For a flat bottom with a constant water depth h, carrier wavenumber $k = k_0$ is also constant as ω; for an uneven bottom, wavenumber k will be changed because of spatial inhomogeneity due to the bottom topography. The change in wave dispersion will also be reflected in the group speed c_g

$$c_g = \frac{g}{2\omega_0}[\sigma + kh(1 - \sigma^2)]. \tag{2.8}$$

In other words, k and c_g are functions of h.

For a weakly nonlinear wave train, the modulation parameter comes from the contribution from the small perturbation in high-order harmonic, so we further expand the velocity potential Φ and free surface elevation η into harmonic functions. In this research, we assume the modulation caused by the nonlinear effect and the depth variations are of the same order of magnitude, referring to Liu & Dingemans (1989). Therefore, we make this small parameter equal to wave steepness ε, and expand Φ and η in the form of

$$\Phi(x, y, z, t) = \sum_{n=1}^{\infty} \varepsilon^n \left[\sum_{m=-n}^{n} \Phi_{nm}(x, y, z, t)E^m\right], \tag{2.9}$$

$$\eta(x, y, t) = \sum_{n=1}^{\infty} \varepsilon^n \left[\sum_{m=-n}^{n} \eta_{nm}(x, y, t)E^m\right], \tag{2.10}$$

$$E = \exp\left\{\mathrm{i}\left[\int^x k(x)\,\mathrm{d}x - \omega_0 t\right]\right\}, \tag{2.11}$$

where E represents the harmonic functions, and the complex conjugates part satisfy $\Phi_{n,-m} = \tilde{\Phi}_{nm}$, $\eta_{n,-m} = \tilde{\eta}_{nm}$. We take $n \leq 3$ in the derivation since ε is very small.

With the expansion of Φ and η to the third order of ε, the method of multiple scales introduced in Davey & Stewartson (1974) is applied to give the solution at different orders and harmonic. The details in this process are similar to Hasimoto & Ono (1972). To simplify the problem, we suppose that the water depth h varies slowly. Additionally, we want to concentrate on the variation of depth in the wave propagation direction, so we assume the magnitude of the gradient of depth change satisfies $h'(x) \sim O(\varepsilon^2)$ and $h'(y) \sim O(\varepsilon^3)$. Considering the expansion form in (2.9) and (2.10), the effect of bottom topography change is only reflected in the third order $O(\varepsilon^3)$ and $h'(y) \sim O(\varepsilon^3)$ is equivalent to $h'(y) = 0$. As for the dispersion relation between wavenumber and frequency, the carrier $\omega = \omega_0$ is still constant since there is no temporal variation, but the carrier wavenumber k changes. Based on the above inference, we can get $k = k(x)$ and $c_g = c_g(x)$ on the principal wave direction, and we can introduce a specific variable substitution of t and x, referring to Djordjević & Redekopp (1978)

$$\tau = \varepsilon \left[\int^x \frac{\mathrm{d}x}{c_g(x)} - t \right], \quad \xi = \varepsilon^2 x, \ \zeta = \varepsilon y. \tag{2.12}$$

We apply (2.12) to transfer (x, y, t) to (ξ, ζ, τ) and put (2.9)–(2.11) into (2.1)–(2.6), then the evolution equation of envelope $\bar{A}(\xi, \zeta, \tau)$ for a very mild slope can be given in the form of

$$\mathrm{i}\beta_h \bar{A} + \mathrm{i}\frac{\partial \bar{A}}{\partial \xi} + \beta_t \frac{\partial^2 \bar{A}}{\partial \tau^2} + \beta_y \frac{\partial^2 \bar{A}}{\partial \zeta^2} = \beta_n |\bar{A}|^2 \bar{A}, \tag{2.13}$$

where

$$\beta_h = \frac{(1-\sigma^2)(1-kh\sigma)}{\sigma + kh(1-\sigma^2)} \frac{\mathrm{d}(kh)}{\mathrm{d}\xi} = \frac{1}{2c_g} \frac{\mathrm{d}(c_g)}{\mathrm{d}\xi}, \tag{2.14a}$$

$$\beta_t = -\frac{1}{2\omega_0 c_g} \left[1 - \frac{gh}{c_g^2}(1-\sigma^2)(1-kh\sigma) \right], \tag{2.14b}$$

$$\beta_y = \frac{1}{2k} \frac{\partial \omega}{\partial k} \equiv \frac{c_g}{2k}, \tag{2.14c}$$

$$\begin{aligned} \beta_n = {} & k^2 \omega_0 \left[\frac{1}{16}(9 - 10\sigma^2 + 9\sigma^4) - \frac{1}{2\sinh^2 2kh} \right] \\ & + \left[\frac{\omega_0^3}{g} \frac{1}{2g}(\sigma^2 - 1) + \frac{k}{c_g} \right] \left(\frac{c_g^2}{c_g^2 - gh} \right) \left[\frac{g^2 k}{2\omega_0 c_g} + \frac{\omega_0^2}{4\sinh(kh)^2} \right]. \end{aligned} \tag{2.14d}$$

Here, β_h represents the contribution from topography change, which is proportional to the derivative of the wavenumber with respect to coordinate ξ. When the topography change becomes very small, $\beta_h \approx 0$ and (2.13) is equivalent to the evolution equation in Davey & Stewartson (1974). Here, β_t and β_y give the local curvature based on the linear dispersion relation for carrier wave period and lateral component of wavenumber, respectively, and β_n represents the contribution from the nonlinear effect due to the quasi-resonant four-wave interaction.

2.2. *Numerical solution and freak wave estimation*

In the 1-D problem of the unidirectional wave train, as in Lyu *et al.* (2021), the evolution equation of $\bar{A}$ is numerically solved in a spatial step by the pseudo-spectral method.

Based on the periodicity of the wave envelop in time and space, the partial differential term in the evolution equation can be transformed into a more concise form by using Fourier transform. In the 1-D problem, we can simplify the partial differential term with respect to time and express it in the frequency domain. In the 2-D problem, the variation in the lateral direction requires the consideration of one more dimension. Based on the periodicity of time and space for a 2-D wavefield, the 2-D Fourier transform is applied to transform (2.13) into an ordinary differential equation

$$\frac{\mathrm{d}\bar{A}}{\mathrm{d}\xi} = -\mathrm{i}\beta_n|\bar{A}|^2\bar{A} - \mathrm{i}\beta_t\omega_\tau^2\bar{A} - \mathrm{i}\beta_y k_\zeta^2\bar{A} - \beta_h\bar{A}, \tag{2.15}$$

where we take the Fourier transformation F_τ with respect to τ on time and F_ζ with respect to ζ on lateral spatial coordinate, respectively, and ω_τ and k_ζ represent corresponding variables about the frequency and the lateral wavenumber in the Fourier transform

$$\dot{A}(\omega_\tau, \xi, \zeta) = F_\tau[\bar{A}(\tau, \xi, \zeta)], \qquad \ddot{A}(\omega_\tau, \xi, k_\zeta) = F_\zeta[\dot{A}(\omega_\tau, \xi, \zeta)]. \tag{2.16}$$

Through the spatial evolution of ξ in (2.15), the wave envelope can be numerically simulated from an initial condition at $\xi = \xi_0$. We assume the initial Fourier amplitude $\ddot{A}(\omega_\tau, \xi_0, k_\zeta)$ satisfies the 2-D Gaussian shape directional spectral

$$\ddot{A}(\omega_\tau, \xi_0, k_\zeta) = \ddot{A}(\omega_\tau, \xi_0, \theta_\zeta) = \frac{a}{2\pi\sigma_\omega\sigma_\theta}\exp\left\{-\frac{1}{2}\left[\left(\frac{\omega_\tau - \omega_0}{\sigma_\omega}\right)^2 + \left(\frac{\theta_\zeta - \theta_0}{\sigma_\theta}\right)^2\right] + \mathrm{i}\psi\right\}, \tag{2.17}$$

where a represents the standard deviation of the envelop and $\varepsilon = ka$, $\theta_\zeta = \arctan(k_\zeta/k_0)$ represents the direction of a single wave with the lateral wavenumber k_ζ, k_0 and ω_0 are carrier wavenumber and frequency, σ_θ is dimensionless directional width, ψ is the random phase uniformly distributed at $[0, 2\pi]$, σ_ω is frequency spectral width and we will also use its dimensionless form $\sigma_s = \sigma_\omega/\omega_0$ in the following discussion. Also, θ_0 is the principal wave direction, and here we set θ_0 is fixed at $\theta_0 = 0$. When $\theta_0 \neq 0$, the incident wave is oblique with the contour line of topography, and wave refraction will occur due to the inhomogeneity of the dispersion relation on the wave front line. This part of the discussion will be given in Part 2.

In this problem, the initial spectrum is decided by the contribution from both the temporal and spatial frequency, and $\ddot{A}$ distributed in a 2-D plane about frequency ω_τ and k_ζ (or θ_ζ). Referring to the 1-D problem as in Janssen (2003), the Benjamin–Feir index (*BFI*) is defined as the ratio between wave steepness ε and dimensionless spectral bandwidth σ_s

$$BFI = \frac{\sqrt{2}\varepsilon}{\sigma_s}. \tag{2.18}$$

In this study, we hope to separate the effect from different contributions in the temporal and spatial parts and concentrate more on the directional dispersion effect, so we continue to use (2.18) as the definition of *BFI* in the initial condition. The parameter σ_θ will be taken as an individual parameter in the spectral bandwidth, and σ_s is set as constant (i.e. σ_ω is constant in (2.17)).

In the principal wave propagation direction, we can solve the wave envelope $\bar{A}$ at each spatial step on x (or ξ) through (2.15), and give the wave surface elevation η by (2.19)

$$\eta(x, y, t) = \varepsilon Re\left[\frac{1}{2}\bar{A}(x, y, t)E\right] + \varepsilon^2 Re\left[\frac{k\cosh kh}{8\sinh^3 kh}(2\cosh^2 kh + 1)\bar{A}^2(x, y, t)E^2\right]. \quad (2.19)$$

Similar to Lyu *et al.* (2021), we integrate $\eta(y, t)$ in (2.19) at each step from offshore to onshore, assuming periodic boundary conditions in time, and construct the surface elevation in a discrete 2-D + T form. Equation (2.19) considers the contribution from first order to second order and second harmonic. The progressive wave is established on the periodicity only in $(\int^x k(x)\,\mathrm{d}x - \omega_0 t)$, because of the contribution of $k_{\zeta 0} = 0$ to the component of lateral length y of the carrier propagating direction.

Because of the very small probability of freak wave occurrence, an ensemble simulation size is necessary to provide a more reliable prediction. In this study, we continue to estimate the nonlinear interaction in wave evolution by the fourth-order moment kurtosis μ_4 and the third-order moment skewness μ_3, and their variation will be compared with the wave height distribution directly obtained from the 2-D + T surface elevation data in a large-size Monte Carlo simulation.

Parameters μ_4 and μ_3 of a fixed point (x_*, y_*) in the wavefield are derived from the discrete surface elevation $\eta(x_*, y_*, t)$ in time series

$$\mu_4 = \frac{Ex(\eta_i - \bar{\eta})^4}{\eta_{rms}^4}, \quad \mu_3 = \frac{Ex(\eta_i - \bar{\eta})^3}{\eta_{rms}^3}, \quad (2.20a,b)$$

where Ex represents expected value, i represents the index number of the data sample, $\bar{\eta}$ is the mean value and η_{rms} is the root mean square value of η. For a wave train in a Gaussian process (i.e. linear random waves), $\mu_4 = 3$ and $\mu_3 = 0$. The theoretical value of μ_4 can be changed with different nonlinear processes or hypotheses. For a narrowband second-order nonlinear wave train, the Stokes wave model gives the contribution from bound waves (Longuet-Higgins 1963). Thus, the values of μ_4 and μ_3 of an estimated inbound wave (marked as μ_4^b, μ_3^b) are related to the wave steepness ε

$$\mu_4^b = 3 + 24\varepsilon^2, \quad \mu_3^b = 3\varepsilon. \quad (2.21a,b)$$

In Janssen (2003) and Mori & Janssen (2006), μ_4 (marked as μ_4^*) can change the quasi-resonant and non-resonant interactions in (2.21). It is parameterized by the fourth-order cumulant κ_{40}, which is proportional to the square of *BFI* defined by Janssen (2003)

$$\mu_4^* = \kappa_{40} + 3, \quad \kappa_{40} = \frac{\pi}{\sqrt{3}}BFI^2. \quad (2.22)$$

Based on the contribution from the quasi-resonant four-wave interactions in (2.22) to wave height H, Mori & Janssen (2006) gave the exceeding probability $P(H)$

$$P(H) = \mathrm{e}^{-H^2/8}\left[1 + \frac{\kappa_{40}}{384}(H^4 - 16H^2)\right], \quad (2.23)$$

and exceeding probability $P_m(H_{max})$ of maximum wave height H_{max}

$$P_m(H_{max}) = 1 - \exp\left\{-N_0\,\mathrm{e}^{-H_{max}^2/8}\left[1 + \frac{\kappa_{40}}{384}(H_{max}^4 - 16H_{max}^2)\right]\right\}, \quad (2.24)$$

where N_0 represents the number of waves in a wave train. Equation (2.24) is well validated by μ_4 in wave tank experiments from Mori *et al.* (2007) and Kashima & Mori (2019).

With the consideration of the directional effect, Mori *et al.* (2011) gave the estimation of maximum κ_{40} with the directional spread σ_θ by

$$\kappa_{40} = \frac{\pi}{\sqrt{3}} BFI^2 \left(\frac{\alpha}{\sigma_\theta} \right), \tag{2.25}$$

where α is an empirical coefficient, and $\alpha = 0.0276$ from their asymptotic analysis in Monte Carlo simulation.

3. Numerical results

3.1. *Model set-up*

With the 2-D Gaussian shape directional spectrum in (2.17) and inverse Fourier transform, we give the initial envelope $\bar{A}(\tau, \xi_0, \zeta)$ in the matrix of time series and the spatial distribution in the lateral direction. As a pseudo-spectral method, discrete Fourier transform requires a sufficient length of the target variable to ensure the result has enough information in the evolution. On the other hand, Fourier transforms for a 2-D matrix require a large amount of time in calculation compared with the 1-D model, which is a critical problem since we apply the Monte Carlo method simulation.

From (2.17), the shape of the initial directional spectrum is decided by the dimensionless spread σ_θ and the frequency spectral width σ_ω. In Lyu *et al.* (2021), the effect from σ_ω has been discussed from the unidirectional wave train with different initial *BFI*. For a 2-D wavefield, the dimensionless spread σ_θ in different sea states varies from 0.15 to 0.5 from research on observations and wave age (Banner & Young 1994; Ewans 1998; Forristall & Ewans 1998). Yuen & Lake (1982) indicated a limitation of the 2-D NLS-like wave model such that the instability of the wave train continually increases in a certain interval, which reflects in our numerical model that the result cannot reach convergence in Monte Carlo simulation when $\sigma_\theta \leq 0.25$. Therefore, we set the $\sigma_\theta = 0.3, 0.4, 0.5$ in the following comparison for different directional spreadings.

To ensure the accuracy and computational efficiency, we make the calculation step constant at $\mathrm{d}\xi = 2 \times 10^{-5} L_0$, where L_0 is carrier wavelength. For the initial condition, carrier angular frequency $\omega = 2.5\ \mathrm{s}^{-1}$, sampling time $\mathrm{d}t = 0.1$ s, time length $L_T = 40T_0$, where T_0 is wave period, and carrier lateral wavenumber $k_{\zeta 0} = 0$, sampling distance $d_y = 0.5L_0$. To ensure that the initial condition given by (2.17) converges to a Gaussian process, we generate the initial Fourier amplitude by a sufficiently large number ($N = L_T/\mathrm{d}t = 1000$) of component waves with different frequencies ω_τ uniformly distributed around the carrier frequency. The kurtosis μ_4 and skewness μ_3 of the initial surface elevation $\eta(x_0, y, t)$ satisfy the Gaussian distribution such that $\mu_4 = 3$ and $\mu_3 = 0$. The initial water depth starts at a medium depth $kh = 5$, wave steepness $\varepsilon = 0.1$. The width of the 2-D computational domain $L_y = 30L_0$ to reflect the propagation of directional waves (the analysis and discussion to decide the appropriate set of d_y and L_y is given in the supplementary materials available at https://doi.org/10.1017/jfm.2023.73). For different forms of bottom topography, the length of the computational domain in the principal direction varies from $30L_0$ to $150L_0$, and the calculation stops at the shallow water $kh = 1.1$, where wave steepness $\varepsilon = 0.1343$. This study assumes the water surface basically maintains the form of a mechanical wave in the evolution, so the wave-breaking case is not taken into consideration. Therefore, our simulation stops before the wave steepness reaches the threshold value of breaking in very shallow water.

Mei & Benmoussa (1984) introduced a normalization to make all parameters dimensionless in the realization process. We apply a different normalization for the variable $(\bar{A}, \xi, \zeta, k_\zeta, \omega_\tau, \tau)$ in programming as follows:

$$A' = \frac{2\pi}{L_0}\bar{A}, \quad \xi' = \frac{2\pi}{L_0}\xi, \quad \zeta' = \frac{2\pi}{\varepsilon L_y}\zeta, \tag{3.1a–c}$$

$$k'_\zeta = \varepsilon\frac{L_y}{2\pi}k_\zeta, \quad \omega' = \varepsilon\frac{L_T}{2\pi}\omega_\tau, \quad \tau' = \frac{2\pi}{\varepsilon L_T}\tau. \tag{3.2a–c}$$

3.2. *Evolution of modulated wave over flat bottoms*

Firstly, we consider the wave evolution over a flat bottom to investigate the effect of initial conditions as reference runs for uneven bottom cases. If we set $\beta_h = 0$, (2.13) is equivalent to the 2-D NLS equation in Davey & Stewartson (1974), and the evolution process is constructed by a spatial step in the principal wave direction. The surface elevation is given in discrete 2-D + T form. In figure 2, we give the transient surface elevation η at $t = 40T_0$ from three random samples with different directional spreads σ_θ and the initial $BFI = 1$ ($\sigma_s = 0.14$) at water depth $kh = 5$. The viewing angle is vertical to the horizontal plane, and we use the colour gradient to represent the elevation. The 2-D irregular waves propagate from the left to the right side, and we can figure out the multi-directions from the wavefront lines. As σ_θ increases from 0.3 to 0.5, the propagation becomes more divergent in different directions, which makes the wavefront appear to be more discontinuous.

The initial condition with a random phase in (2.17) helps generate an irregular wave train, and a Monte Carlo simulation is conducted. For a domain in strict-sense stationary (SSS), the statistical properties remain invariant to any shift at any order, and the surface elevation for a 2-D irregular wave at a fixed point will be generally closed to a zero-mean SSS process when the Monte Carlo simulation for random wave phase has enough ensemble size. In this study, we set the ensemble size to 300 and give the average value of kurtosis μ_4 and skewness μ_3 in time series to each space node. The deciding process of the ensemble size is also discussed in the supplementary materials.

The result in 2-D form can be modified into 1-D form by being averaged again in one space dimension because the statistical significance is uniformly distributed in this 2-D domain. To show the wave evolution process, we take the averaged value on the lateral direction of the principal wave direction and give the Monte Carlo result of the unidirectional wave train and the 2-D wavefield with initial $BFI = 0.5$ ($\sigma_s = 0.28$) for a flat bottom $kh = 7$ to discuss the effect from the directional spread σ_θ in figure 3. The result in the unidirectional wave train can be regarded as $\sigma_\theta = 0$. As σ_θ increases, both kurtosis μ_4 and skewness μ_3 decrease, which implies the increase of directional spreading disperses the nonlinear interactions in the wave train.

For the 2-D propagation in a directional wavefield, both short-time and long-time behaviour of κ_{40} for a narrowband wave train is related to the directional width and a frequency width (Janssen & Bidlot 2009). We are also interested in the kurtosis distribution at the intermediate stages in freak wave forecasting. Mori *et al.* (2011) conducted an asymptotic analysis of κ_{40}, BFI and σ_θ by numerical simulation, and gave (2.25) with empirical coefficient α. Table 1 shows the ensemble-averaged result of the expected maximum κ_{40} and mean κ_{40} at $x \in [20L_0, 30L_0]$ from Monte Carlo simulation of the wave model in this study, and gives the empirical coefficients α_{max} and α_{mean} by (2.25) for maximum κ_{40} and mean κ_{40}, respectively. Due to different calculation conditions, we give different empirical coefficients from Mori *et al.* (2011) ($\alpha = 0.0276$), and the

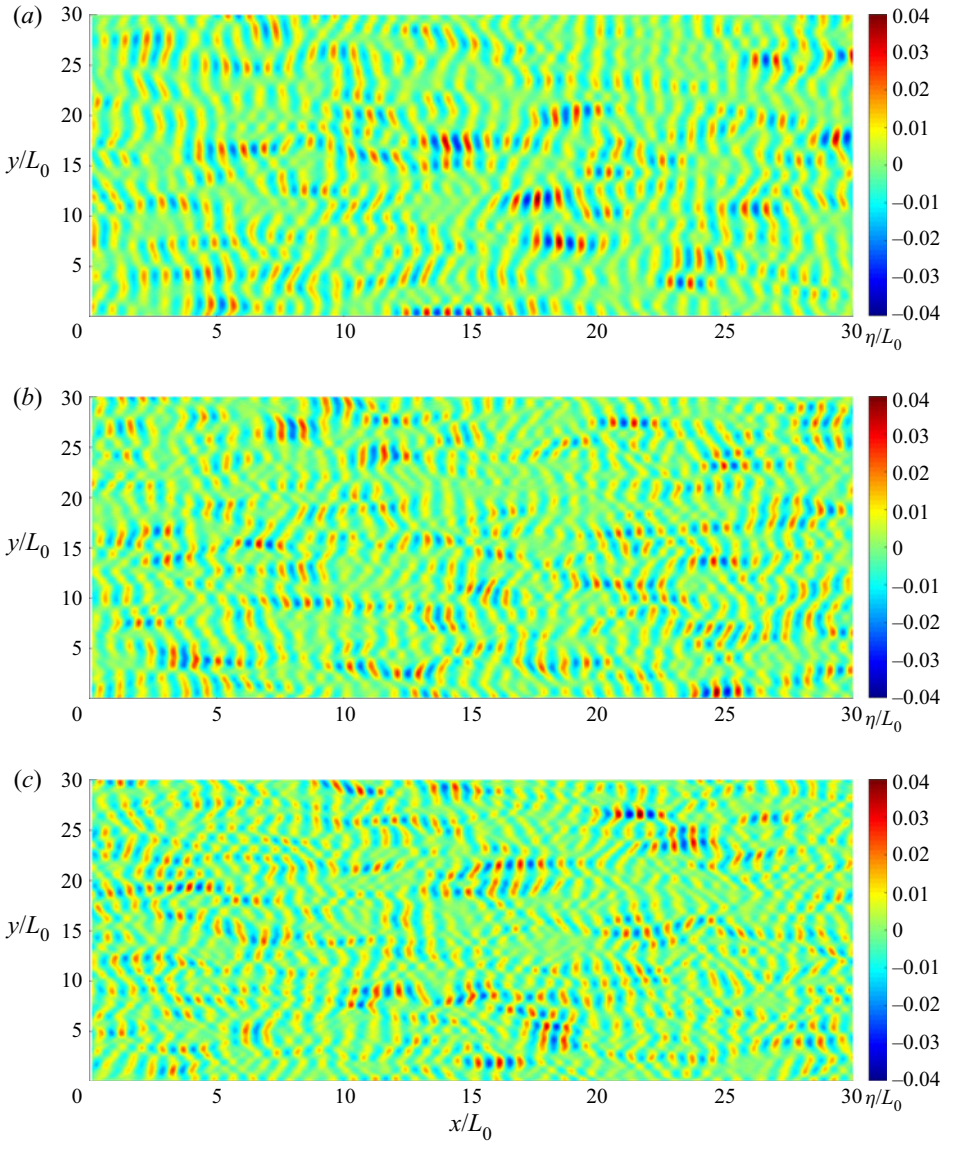

Figure 2. Transient surface elevation η at $t = 40T_0$ from different directional spreads σ_θ with initial $BFI = 1$, $kh = 5$. (*a*) $\sigma_\theta = 0.3$, (*b*) $\sigma_\theta = 0.4$ and (*c*) $\sigma_\theta = 0.5$.

expected maximum κ_{40} is significantly larger than their prediction. Nevertheless, the result from $kh = 7$ shows that the increase of σ_θ and the decrease of BFI lead to the decrease of both maximum and mean κ_{40}, but the change in empirical coefficient α represents that κ_{40} is not strictly inversely proportional to σ_θ as in (2.25), and the case from different initial BFI will ask for a different α. The value of α_{mean} for mean κ_{40} at $kh = 7$ is better than α_{max} to describe the kurtosis of the wavefield, and its value is around 0.09∼0.14. When the water depth becomes shallow ($kh = 5$, 3, 1.1), (2.25) is no longer applicable and α_{mean} and α_{max} significantly decrease. For $kh = 1.1$, the increase of σ_θ leads to the increase of κ_{40} and α_{mean}, which seems anomalous. The behaviour of κ_{40} further indicates

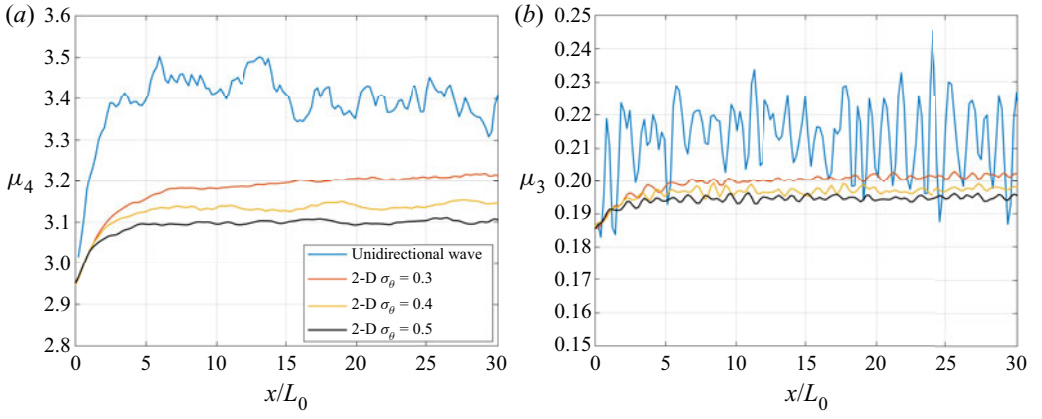

Figure 3. Spatial evolution of kurtosis μ_4 and skewness μ_3 of surface elevation from directional spread σ_θ with initial $BFI = 0.5$, $kh = 7$ (1-D ($\sigma_\theta = 0$), blue; 2-D: red, $\sigma_\theta = 0.3$; yellow, $\sigma_\theta = 0.4$; black, $\sigma_\theta = 0.5$). (*a*) Kurtosis μ_4 and (*b*) skewness μ_3.

kh	σ_θ	Initial BFI	Max κ_{40}	Mean κ_{40}	α_{max}	α_{mean}
7.0	0.3	0.5	6.329	0.180	4.187	0.119
7.0	0.4	0.5	4.555	0.127	4.018	0.112
7.0	0.5	0.5	4.206	0.092	4.638	0.101
7.0	0.6	0.5	3.841	0.064	5.082	0.085
7.0	0.3	0.4	4.441	0.136	4.591	0.141
7.0	0.5	0.4	3.725	0.083	6.418	0.143
5.0	0.3	0.4	3.976	0.117	4.110	0.121
5.0	0.5	0.4	3.368	0.070	5.803	0.121
3.0	0.3	0.4	3.148	0.065	3.254	0.067
3.0	0.5	0.4	2.948	0.038	5.079	0.066
1.1	0.3	0.4	2.294	0.059	2.371	0.061
1.1	0.5	0.4	2.754	0.113	4.745	0.195

Table 1. The ensemble-averaged κ_{40} dependence on BFI and σ_θ at different kh.

that the occurrence of extreme wave height in medium and shallow water cannot only be predicted by the four-wave interaction as in deep water. The contribution from water depth becomes important, especially in shallow water, and the simulation over a changing depth may reveal this process more effectively.

3.3. *Evolution of modulated wave over uneven bottoms*

This section considers Monte Carlo simulation of the 2-D wave model for uneven bottoms. The variation in the bottom topography brings about the spatial inhomogeneity in the dispersion, which reflects in both second-order and third-order effects. Our numerical model by (2.13) assumes the depth mildly changes in the principal wave direction, and the bottom topography does not vary in its lateral direction. Therefore, the statistical properties remain stationary on the y-axis but vary on the x-axis.

As a simulation of the bottom topography from offshore to onshore, we set the depth to slowly decrease from a medium-water depth to shallow water. In previous research (e.g. Kashima & Mori 2019; Li *et al.* 2021; Lyu *et al.* 2021), the abrupt change in depth or

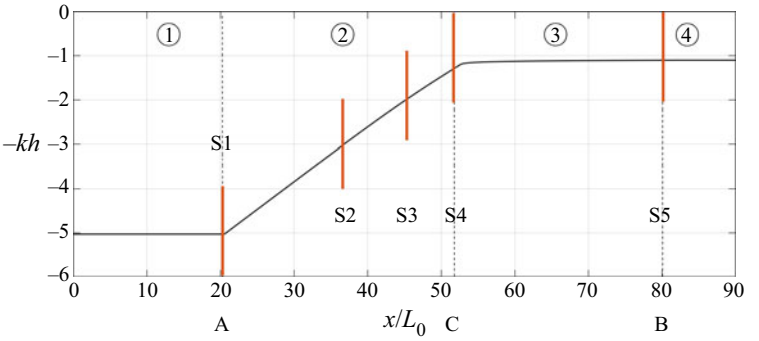

Figure 4. The variation of water depth kh on the bottom topography with $\gamma_s = 0.02$.

slope led to significant local peaks in μ_3 and μ_4 due to the after effect. Usually, the water depth decreases in a smoother way in the natural seabed. On the other hand, the local peak caused by this unusual topography is so significant that it may cover the difference caused by the directional effect. To make our simulation closer to the natural seabed, we adjust the sloping region in figure 1 between A and B to become smoother and to continuously decrease, as shown in figure 4. The sloping region is divided into two parts by the dividing line C at $kh = 1.2$: the depth linearly decreases with a slope γ_s from $kh = 5$ to $kh = 1.2$; the depth decreases with a decaying slope $\gamma_s' = \gamma_s(h/1.55)^{40}$ from $kh = 1.2$ to $kh = 1.1$. In the shallow-water area, the derivative of the decreasing depth is approximately continuous, and we set $\gamma_s = 0.05, 0.02, 0.01$ to ensure the depth changes very mildly under the assumption $h'(x) \sim O(\varepsilon^2)$.

Figures 5 and 6 shows the averaged values of kurtosis and skewness from the Monte Carlo simulation of the bottom type in figure 4. In figure 5, we give the averaged kurtosis μ_4 in 2-D form at the different directional spread σ_θ and slope angle γ_s with initial $BFI = 0.4$ ($\sigma_s = 0.35$). Comparing the result from different σ_θ in figure 5(*a–c*), we find that μ_4 decreases in the deep-water depth but increases in the shallow water when the initial directional spreading σ_θ increases from 0.3 to 0.5, which shows that the same phenomenon results in a flat bottom in § 3.1. In the medium-water depth region between locations A and C, μ_4 decreases with the decrease of water depth, and it rebounds at the end of the constant sloping region (location C) where $kh = 1.2$. In the region between C and B, where the slope angle mildly decreases, μ_4 decreases and becomes stable at the same level as the final flat bottom in shallow water $kh = 1.1$. The evolution of μ_4 indicates that the directional dispersion effect decreases the occurrence probability of freak waves in deep and medium water but increases it in shallow water. As the wave propagates from the medium water to shallow water, the wave evolution is significantly affected by the bottom topography, and the 1-D result in figure 5(*d*) clearly gives the rebound of μ_4 due to the slope angle. To further study the effect from the bottom topography, we give the mean μ_4 at $\gamma_s = 0.02$ and $\gamma_s = 0.01$ with initial $BFI = 0.4$ and $\sigma_\theta = 0.3$ in figures 5(*e*) and 5(*f*). The result shows that the rebound of μ_4 decreases as the bottom change become milder, and figure 5(*g*) provides the variation of μ_4 in the principal wave direction in one dimension. Comparing μ_4 over uneven bottoms between the unidirectional wave train and the 2-D wavefield, we find the slope angle similarly affects the wave evolution. However, its contribution is more significant in two dimensions due to the dispersion effect in the four-wave interaction, which implies the second-order effect plays a more important role in a directional 2-D wavefield.

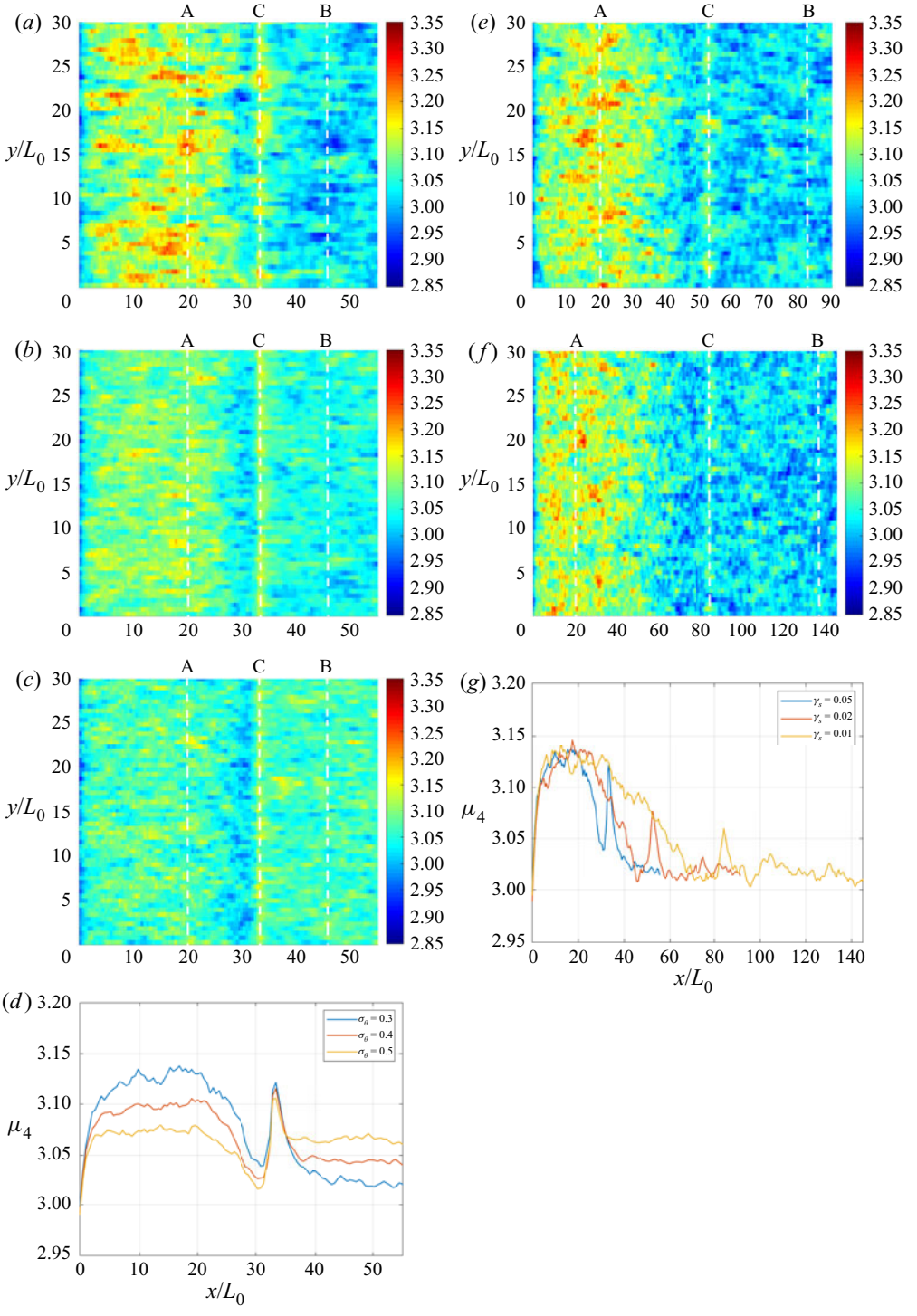

Figure 5. Mean kurtosis of surface elevation η for uneven bottoms at different directional spreads σ_θ and slope angles γ_s with initial $BFI = 0.4$ (blue, $\sigma_\theta = 0.3$; red, $\sigma_\theta = 0.4$; yellow, $\sigma_\theta = 0.5$; g: blue, $\gamma_s = 0.05$; red, $\gamma_s = 0.02$; yellow, $\gamma_s = 0.01$). (*a*) $\sigma_\theta = 0.3$, $\gamma_s = 0.05$, (*b*) $\sigma_\theta = 0.4$, $\gamma_s = 0.05$, (*c*) $\sigma_\theta = 0.5$, $\gamma_s = 0.05$, (*d*) $\sigma_\theta = 0.3$, 0.4, 0.5, $\gamma_s = 0.05$, (*e*) $\sigma_\theta = 0.3$, $\gamma_s = 0.02$, (*f*) $\sigma_\theta = 0.3$, $\gamma_s = 0.01$ and (*g*) $\sigma_\theta = 0.3$, $\gamma_s = 0.05$, 0.02, 0.01.

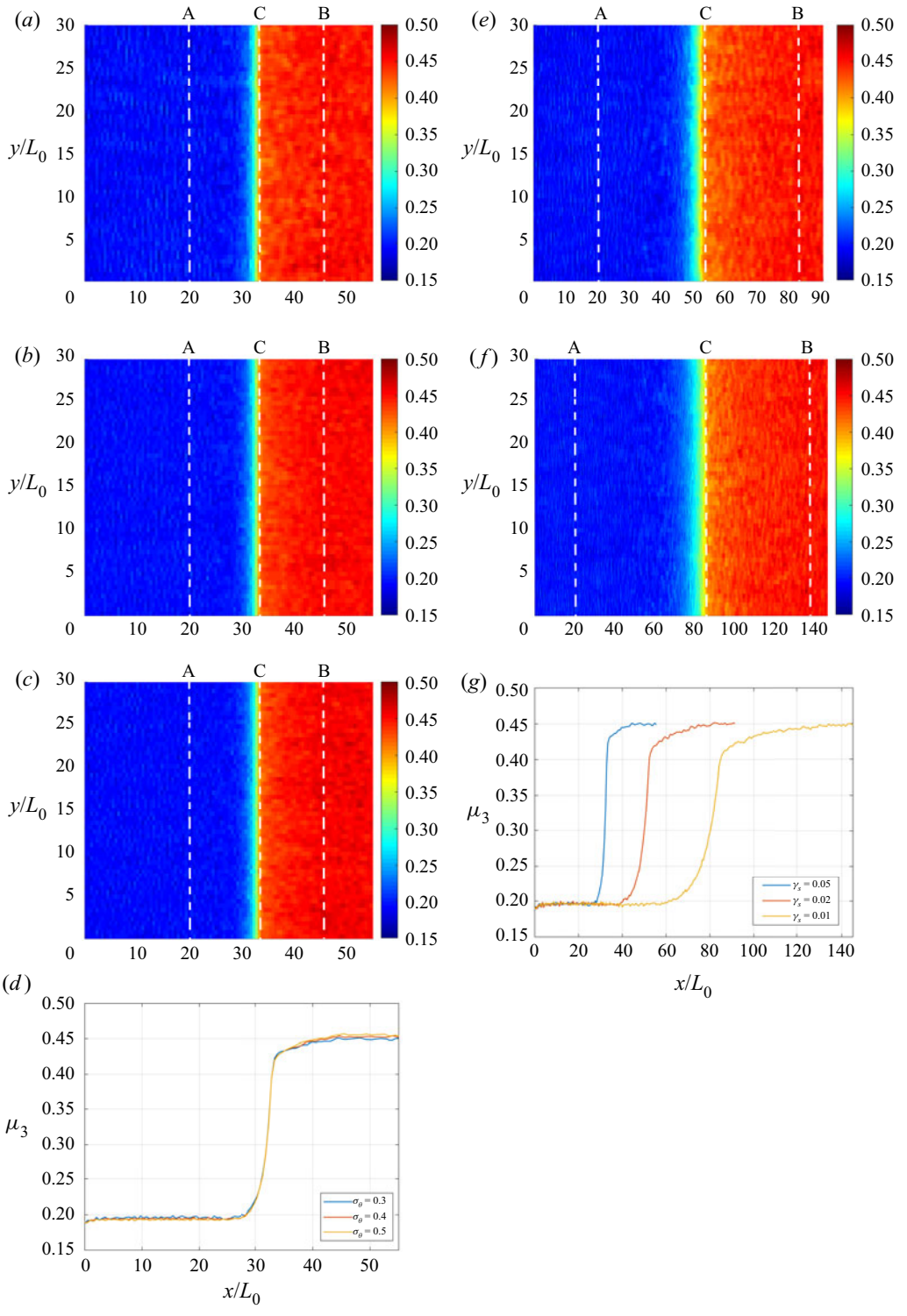

Figure 6. Mean skewness of surface elevation η for uneven bottoms at different directional spreads σ_θ and slope angles γ_s with initial $BFI = 0.4$ (blue, $\sigma_\theta = 0.3$; red, $\sigma_\theta = 0.4$; yellow, $\sigma_\theta = 0.5$; g: blue, $\gamma_s = 0.05$; red, $\gamma_s = 0.02$; yellow, $\gamma_s = 0.01$). (*a*) $\sigma_\theta = 0.3$, $\gamma_s = 0.05$, (*b*) $\sigma_\theta = 0.4$, $\gamma_s = 0.05$, (*c*) $\sigma_\theta = 0.5$, $\gamma_s = 0.05$, (*d*) $\sigma_\theta = 0.3,\ 0.4,\ 0.5$, $\gamma_s = 0.05$, (*e*) $\sigma_\theta = 0.3$, $\gamma_s = 0.02$, (*f*) $\sigma_\theta = 0.3$, $\gamma_s = 0.01$ and (*g*) $\sigma_\theta = 0.3$, $\gamma_s = 0.05, 0.02, 0.01$.

In figure 6, we give skewness μ_3 in the same form as μ_4 in figure 5 at the same condition. Different from μ_4, μ_3 does not influence directional spread from figure 6(*a–d*) due to the unchanging second-order nonlinear interaction. When the bottom topography changes, figure 6(*e–g*) shows that μ_3 increases as the water depth become shallow. This process will slow down if the slope angle becomes mild, but it only means μ_3 is determined by the water depth kh and the change from slope angle γ_s has little influence. Different from the unidirectional wave train, μ_3 in the 2-D wavefield is basically only determined by the variation in dispersion due to depth change, and is hardly affected by the local bathymetry effect. When the wave trains propagate into shallow water, μ_3 increases with the increase of wave steepness ε.

3.4. *Quantitative analysis of the extreme wave height*

In §§ 3.2 and 3.3, the evolutions of the nonlinear resonant interactions have been discussed with the bathymetry effect at different water depths. Parameters μ_4 and μ_3 represent different nonlinear mechanisms, and they show different characteristics on the directional wavefield over an uneven bottom. However, the final result of the occurrence of extreme wave height is their combined effect, and we cannot simply give the estimation until giving a quantitative analysis of the distribution of surface elevation η.

In figure 7, we give the expected maximum wave height H_{max} and maximum wave crest η_{max} in the principal wave direction. In the same form as μ_4 and μ_3 in figures 5 and 6, H_{max} and η_{max} are counted from the time series sampling data at a fixed point in the 2-D wavefield, and their ensemble-averaged value is given by Monte Carlo simulation. We make the wave height dimensionless by taking H_{max}/η_{rms} and η_{max}/η_{rms}, and continue to write them as H_{max} and η_{max} for convenience. The result contains the wave train with different directional spreadings $\sigma_\theta = 0.3$, 0.4, 0.5 over the bottom topography $\gamma_s = 0.05$, 0.02, 0.01, and the theoretical result from the linear model (Rayleigh distribution) and the numerical result from the second-order bound wave model in $\sigma_\theta = 0.3$, $\gamma_s = 0.05$ are given for comparison. The Rayleigh distribution can be referred to as the standard linear narrow-banded wave theory in Goda (1970, 2000), in which the wave height H follows the Gaussian distribution and the exceeding probability $P_m(H_{max})$ follows

$$P_m(H_{max}) = 1 - \exp(-N_0\, \mathrm{e}^{-H_{max}^2/8}), \tag{3.3}$$

where the number of waves $N_0 = 40$ in our simulation. From deep water to shallow, H_{max} in 2-D model monotonically decreases with the water depth in comparison with the second-order model. Similar with μ_4, the peak of H_{max} is suppressed by the increase of σ_θ in deep water but is enhanced in shallow water. However, there is no significant change in the slope. In figure 7(*b*), the η_{max} significantly increases in shallow water, and the local peak reflects the contribution from the slope. Even when the bottom changes in a relatively continuous process, this local peak still occurs, and is consistent with the variation of μ_4. Different from H_{max} in shallow water, the increase of η_{max} is related to μ_3, in keeping with the general deformation of waves in the shoaling process. In the Rayleigh distribution, H_{max} and η_{max} are independent of the bathymetry. The linear model underestimates H_{max} in deep water and overestimates it in the shallow water, and significantly underestimates η_{max}. As a result of the second-order bound wave model, H_{max} is hardly affected by the bottom topography and η_{max} is determined by wave steepness. Comparing different models, the present model provides more consideration of the different effects of the four-wave interaction at various depths. Comparing the result in figures 5–7, we find the

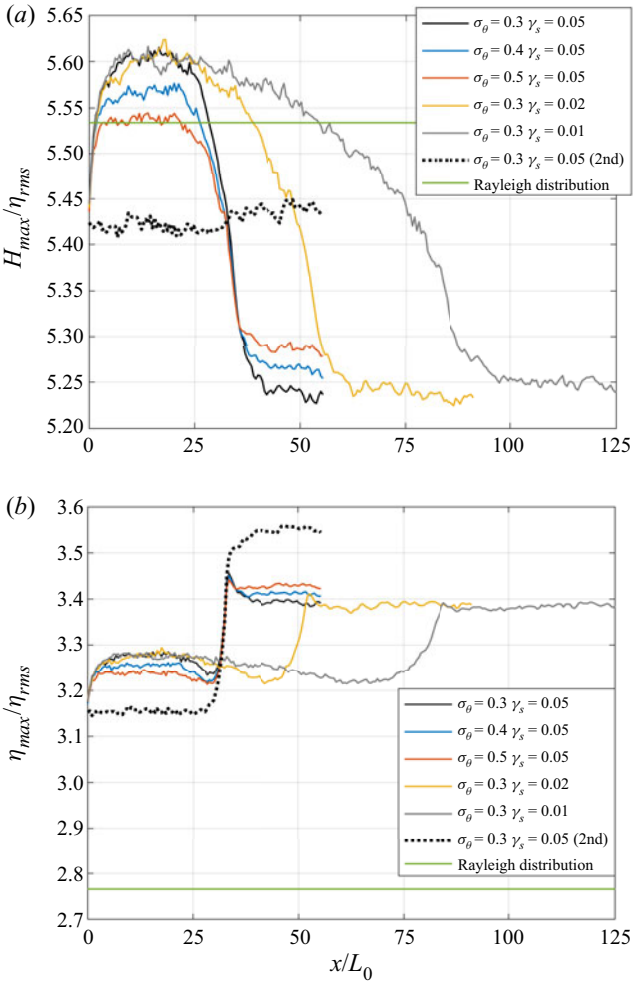

Figure 7. Ensemble-averaged expected maximum wave height and free surface elevation distribution at initial $BFI = 0.4$ from different σ_θ and γ_s (present model: black, $\sigma_\theta = 0.3\ \gamma_s = 0.05$; blue, $\sigma_\theta = 0.4\ \gamma_s = 0.05$; red, $\sigma_\theta = 0.5\ \gamma_s = 0.05$; yellow, $\sigma_\theta = 0.3\ \gamma_s = 0.02$; grey, $\sigma_\theta = 0.3\ \gamma_s = 0.01$. Second-order model: dotted, $\sigma_\theta = 0.3\ \gamma_s = 0.05$. Rayleigh distribution: green line). (*a*) Maximum wave height H_{max} and (*b*) maximum wave crest η_{max}.

rebound of μ_4 at location C does not reflect in H_{max} but shows in η_{max}, which implies the wave height distribution at this area is more determined by the topography effect at second order rather than the four-wave interaction at third order.

When concentrating on the freak wave problem, only the expected value is insufficient to estimate the extreme case. Therefore, we integrate the distributions of H_{max} and η_{max} at each section in the principal wave direction. If we follow the common definition of the freak wave as the wave height exceeds the significant wave height by a factor two, then the occurrence probability of a freak wave height is $P_f(H_{max})$ when $H_{max} > 8\eta_{rms}$ and the corresponding probability estimated by the wave crest is $P_f(\eta_{max})$ when $\eta_{max} > 4\eta_{rms}$ under the standard linear narrow-banded wave theory from Goda (1970, 2000) (*f*, freak wave). Figure 8 calculates the probabilities as mentioned above and gives the fit curves through the tenth-order polynomial. A little different from figures 5–7, the horizontal

axis is set to be the water depth kh in figure 8, so we can more easily check the effect from different γ_s at the same depth. In figure 8(a), $P_f(H_{max})$ monotonically decreases with the water depth as expected H_{max}, but more details can be given: in relatively deep water such as $kh > 4$, the convergence of $P_f(H_{max})$ becomes worse, which implies the variance of surface elevation significantly rises; for the shallow water $kh < 2$, the increase of slope angle γ_s enhances the probability of freak waves; the directional spreading σ_θ plays a more important role in deep water, but bottom topography has a greater impact in shallow water. Compared with figure 8(a), $P_f(H_{max})$ in figure 8(b) is much larger than $P_f(H_{max})$ in general, and it experiences a process of descending, ascending and descending again with the decrease of kh. In the linear model, the probabilities in figure 8(a,b) show the same result, and their deviation from current models corresponds to the evolution in figure 7. The result from the second-order bound wave model continues to show a strong correlation with wave steepness ε, and it gives an abnormal enhancement in both $P_f(H_{max})$ and $P_f(\eta_{max})$ in very shallow water after the slope section, which is not consistent with the natural state and experiments.

In figures 9 and 10, we give the wave height distribution in CDF in logarithmic coordinates at specific sections at different water depths. We choose five sections on the sloping region in figure 4: S1 (dashed line A in previous figures) where $kh = 5$; S2 where $kh = 3$; S3 where $kh = 2$; S4 (dashed line C in previous figures) where $kh = 1.2$; S5 (dashed line B in previous figures) where $kh = 1.1$. Figure 9 shows the CDF of $P_m(H_{max})$ from the same conditions as before compared with the Rayleigh distribution (i.e. linear distribution). As the water depth decreases from S1 to S5, the occurrence probability of H_{max} decreases from the comparison with the Rayleigh distribution (the linear distribution model does not change with water depth). The nonlinear model gives a higher exceeding probability of extreme events than the linear distribution in deep water (S1) but lower in shallow water (S4, S5). They have a similar prediction of wave heights distribution in medium-water depth (S2, S3). In S1–S3, the increase of directional spread σ_θ leads to the decrease in the probability of exceeding $H_{max}/\eta_{rms} > 6$. However, in shallow-water depth (S4, S5), the effect of σ_θ is very limited or even becomes opposite. The effect from γ_s works mainly in the shallow region, and focuses on the distribution of larger values (i.e. the occurrence of a 'freak wave'). The result from the second-order bound wave model is hardly affected by the water depth from S1 to S4, but increases in very shallow water S5, especially for the occurrence of extreme values, and exceeds the result from the present model. In figure 10, we give the CDF of $P_m(\eta_{max})$ in the same form. Basically, $P_m(\eta_{max})$ shows a similar variation as $P_m(H_{max})$ under the effect from σ_θ and γ_s, but $P_m(\eta_{max})$ markedly exceeds the Rayleigh distribution, which indicates that the wave deformation makes the wave crest exceed half the wave height due to the nonlinear effect. In shallow water, this deviation becomes more obvious for a smaller value $\eta_{max}/\eta_{rms} > 3$, even the extreme case decreases, which indicates the second-order nonlinear effect significantly rises due to the bottom topography change.

4. Conclusion

Based on the 2-D dNLS equation and pseudo-spectral method, we establish a third-order nonlinear model for the evolution of the directional wave train in a 2-D wavefield for an uneven bottom. With Monte Carlo simulation from random initial phase information, we summarize the nonlinear effect from four-wave interaction and spatial inhomogeneity and the dispersion from directional spreading in the wave evolution through the statistical features of random irregular waves.

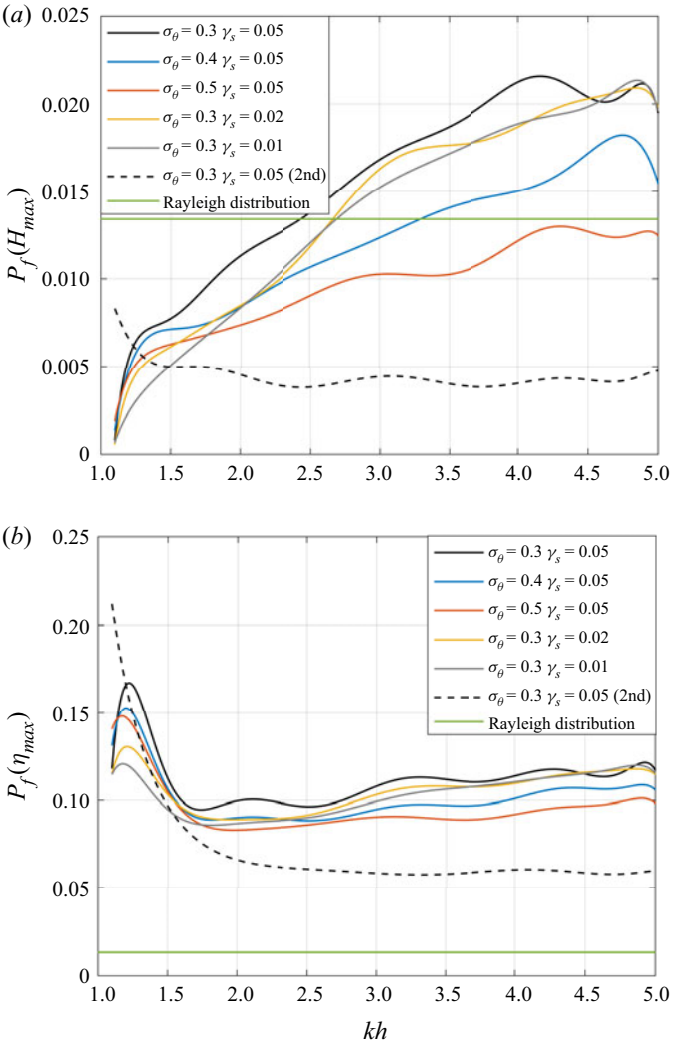

Figure 8. Occurrence probability of the freak wave in wave height and free surface elevation distribution at initial $BFI = 0.4$ from different σ_θ and γ_s (present model: black, $\sigma_\theta = 0.3$ $\gamma_s = 0.05$; blue, $\sigma_\theta = 0.4$ $\gamma_s = 0.05$; red, $\sigma_\theta = 0.5$ $\gamma_s = 0.05$; yellow, $\sigma_\theta = 0.3$ $\gamma_s = 0.02$; grey, $\sigma_\theta = 0.3$ $\gamma_s = 0.01$. Second-order model: dotted, $\sigma_\theta = 0.3$ $\gamma_s = 0.05$. Rayleigh distribution: green line). (*a*) probability of $H_{max} > 8\eta_{rms}$ and (*b*) probability of $\eta_{max} > 4\eta_{rms}$.

To investigate the occurrence of the freak wave in different conditions, we discuss the contribution to the nonlinear interactions from different mechanisms and hypotheses, and compare the distribution of extreme wave height and crest to find the essential factor. The result indicates the following:

(i) Compared with the unidirectional wave, the directional spreading in the 2-D wavefield significantly affects the wave train evolution and the occurrence of freak waves. The rise of the directional dispersion will make the kurtosis decrease in deep water but increase in shallow water. Correspondingly, the directional spread contributes to the exceedance probability of maximum wave height and crest, the same as kurtosis.

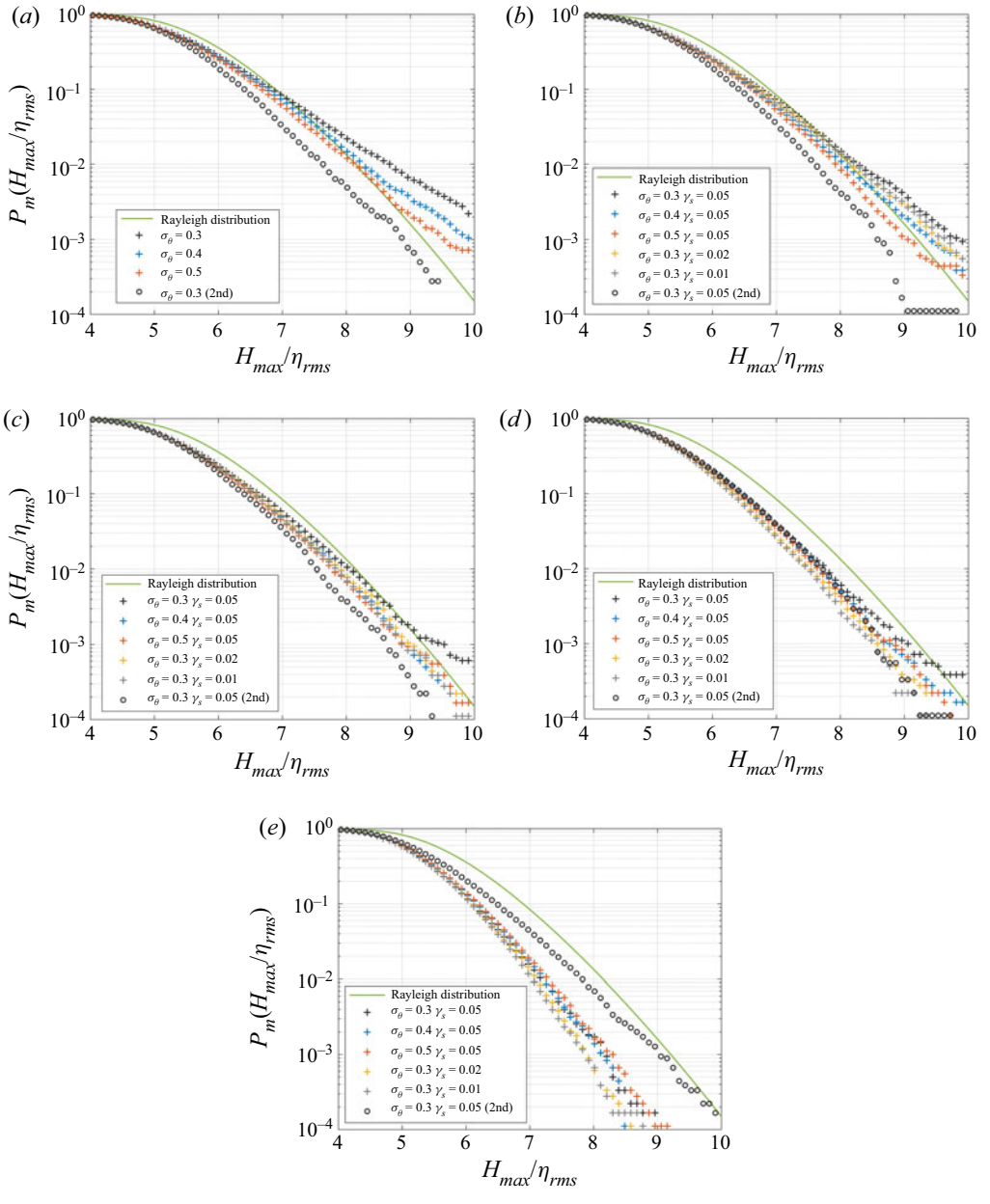

Figure 9. Exceedance probability of maximum wave height H_{max} at initial $BFI = 0.4$ from different σ_θ and γ_s (present model: black cross, $\sigma_\theta = 0.3\ \gamma_s = 0.05$; blue, $\sigma_\theta = 0.4\ \gamma_s = 0.05$; red, $\sigma_\theta = 0.5\ \gamma_s = 0.05$; yellow, $\sigma_\theta = 0.3\ \gamma_s = 0.02$; grey, $\sigma_\theta = 0.3\ \gamma_s = 0.01$. Second-order model: black circle, $\sigma_\theta = 0.3\ \gamma_s = 0.05$. Rayleigh distribution: green line); (*a*) S1 ($kh = 5$), (*b*) S2 ($kh = 3$), (*c*) S3 ($kh = 2$), (*d*) S4 ($kh = 1.2$) and (*e*) S5 ($kh = 1.1$).

(ii) The directional dispersion effect has almost no effect on the skewness of surface elevation at second order, and the wave steepness mainly determines the skewness in a 2-D wavefield.

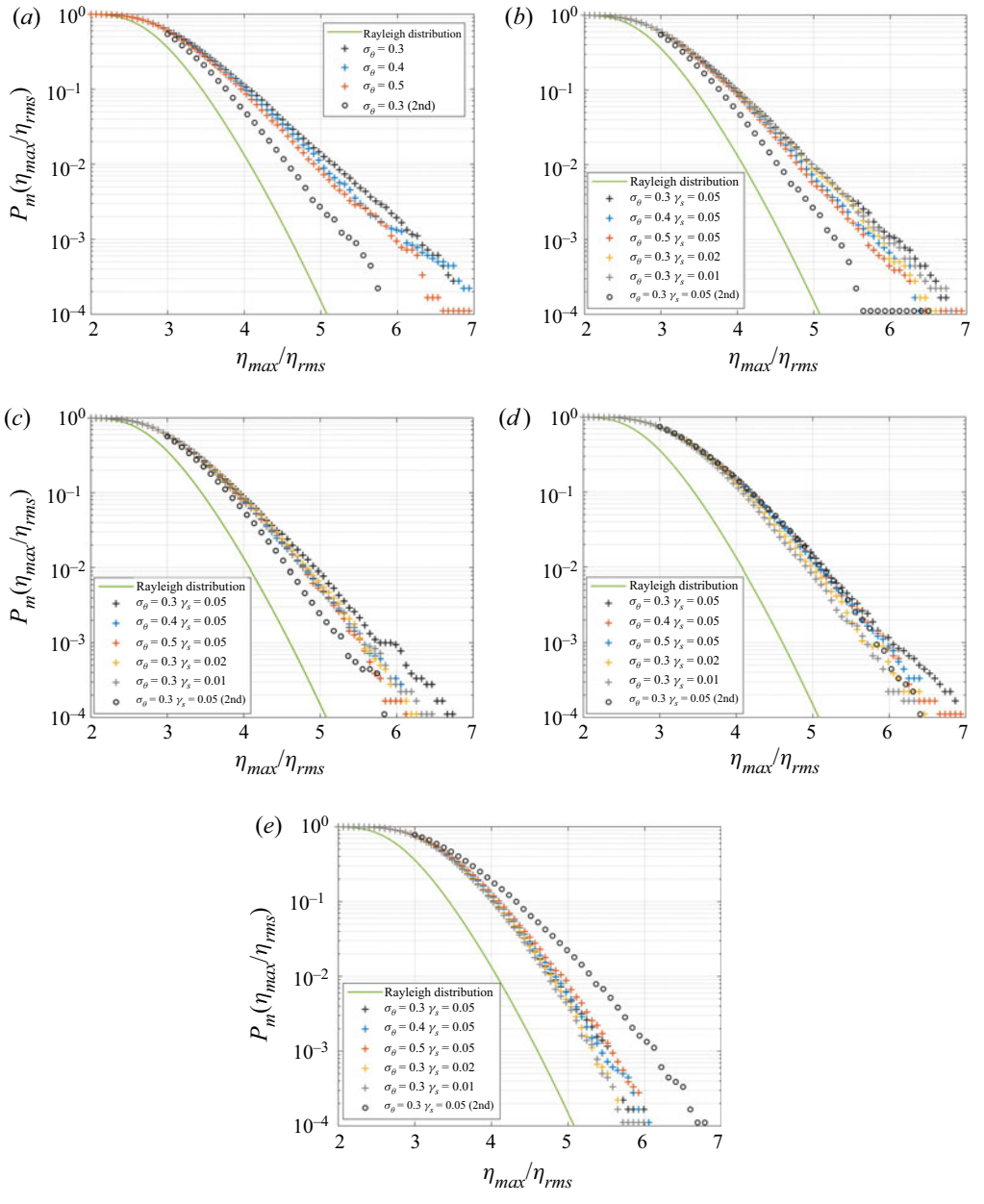

Figure 10. Exceedance probability of maximum wave crest η_{max} at initial $BFI = 0.4$ from different σ_θ and γ_s (present model: black cross, $\sigma_\theta = 0.3\ \gamma_s = 0.05$; blue, $\sigma_\theta = 0.4\ \gamma_s = 0.05$; red, $\sigma_\theta = 0.5\ \gamma_s = 0.05$; yellow, $\sigma_\theta = 0.3\ \gamma_s = 0.02$; grey, $\sigma_\theta = 0.3\ \gamma_s = 0.01$. Second-order model: black circle, $\sigma_\theta = 0.3\ \gamma_s = 0.05$. Rayleigh distribution: green line); (*a*) S1 ($kh = 5$), (*b*) S2 ($kh = 3$), (*c*) S3 ($kh = 2$), (*d*) S4 ($kh = 1.2$) and (*e*) S5 ($kh = 1.1$).

(iii) In shallow water, a steep slope angle leads to the local peak of kurtosis due to wave shoaling. Correspondingly, it reflects in the increase of the exceedance probability of maximum wave height and crest.

(iv) Regarding the degree of impact, the dispersion effect from directional spread mainly affects the wave evolution and the occurrence of the freak wave in deep water. However, the bottom topography change becomes the major role in the medium and shallow water before wave breaking.

The model allows a weakly oblique incident wave angle to the slope. The oblique wave case will be given in the near future.

It should be pointed out that this model still needs to be improved due to the following limitations: first, the wave breaking in shallow-water depth is not taken into consideration; second, the bottom topography is idealized, which ignores the variation on the lateral direction and restricts the slope in a relatively mild range about the steepness squared. Additionally, the wavefield in this study is of sufficiently narrow-banded spectrum. To apply the results of this manuscript to field data, we also need to consider the contribution from the bandwidth of the spectrum to the distribution of wave height and crest height (e.g. Næss 1985). Furthermore, we assume that there is no extra contribution to the wave evolution during its propagation processes, such as wind or current, so the initial conditions and bottom topography only decide the directional spreading.

Supplementary material. Supplementary material are available at https://doi.org/10.1017/jfm.2023.73.

Acknowledgements. Z.L. wishes to thank MEXT. Scholarship of Japan and N.M. appreciates for Grants-in-Aid for Scientific Research KAKENHI (19H00782) by JSPS for providing necessary support.

Declaration of interests. The authors report no conflict of interest.

Author ORCIDs.
Zuorui Lyu https://orcid.org/0000-0002-4683-812X;
Nobuhito Mori https://orcid.org/0000-0001-9082-3235.

References

Alber, I. & Saffman, P. 1978 Stability of random nonlinear deep-water waves with finite bandwidth spectra. *T.R.W., Defense and Space System Group Tech*, *Rep.* 31326-6035-RU-00.

Banner, M.L. & Young, I.R. 1994 Modeling spectral dissipation in the evolution of wind waves. *J. Phys. Oceanogr.* **24** (7), 1550–1571.

Benjamin, T.B. 1967 Instability of periodic wavetrains in nonlinear dispersive systems. *Proc. R. Soc. Lond. Ser.* A*, Math. Phys. Sci.* **299** (1456), 59–76.

Benney, D.J. & Roskes, G.J. 1969 Wave instabilities. *Stud. Appl. Maths* **48** (4), 377–385.

Bolles, C.T., Speer, K. & Moore, M.N.J. 2019 Anomalous wave statistics induced by abrupt depth change. *Phys. Rev. Fluids* **4** (1), 011801.

Davey, A. & Stewartson, K. 1974 On three-dimensional packets of surface waves. *Proc. R. Soc. Lond.* A*, Math. Phys. Sci.* **338** (1613), 101–110.

Djordjević, V.D. & Redekopp, L.G. 1978 On the development of packets of surface gravity waves moving over an uneven bottom. *Z. Angew. Math. Phys.* **29** (6), 950–962.

Draper, L. 1965 'Freak' ocean waves. *Mar. Observer* **35**, 193–195.

Ewans, K.C. 1998 Observations of the directional spectrum of fetch-limited waves. *J. Phys. Oceanogr.* **28** (3), 495–512.

Forristall, G.Z. & Ewans, K.C. 1998 Worldwide measurements of directional wave spreading. *J. Atmos. Ocean. Technol.* **15** (2), 440–469.

Goda, Y. 1970 Numerical experiments on wave statistics with spectral simulation. *Rep. Port Harbour Res. Inst.* **9**, 3–57.

Goda, Y. 2000 *Random Seas and Design of Maritime Structures*, 2nd edn. World Scientific.

Gramstad, O. & Trulsen, K. 2007 Influence of crest and group length on the occurrence of freak waves. *J. Fluid Mech.* **582**, 463–472.

Gramstad, O., Zeng, H., Trulsen, K. & Pedersen, G.K. 2013 Freak waves in weakly nonlinear unidirectional wave trains over a sloping bottom in shallow water. *Phys. Fluids* **25** (12), 122103.

Hasimoto, H. & Ono, H. 1972 Nonlinear modulation of gravity waves. *J. Phys. Soc. Japan* **33** (3), 805–811.

JANSSEN, P.A.E.M. 2003 Nonlinear four-wave interactions and freak waves. *J. Phys. Oceanogr.* **33** (4), 863–884.

JANSSEN, P.A.E.M. & BIDLOT, J.R. 2009 On the extension of the freak wave warning system and its verification. *Memo*. 588. European Centre for Medium-Range Weather Forecasts.

KASHIMA, H., HIRAYAMA, K. & MORI, N. 2014 Estimation of freak wave occurrence from deep to shallow water regions. *Coast. Engng Proc.* **1** (34), 36.

KASHIMA, H. & MORI, N. 2019 Aftereffect of high-order nonlinearity on extreme wave occurrence from deep to intermediate water. *Coast. Engng* **153**, 103559.

KIMMOUN, O., HSU, H.-C., HOFFMANN, N. & CHABCHOUB, A. 2021 Experiments on unidirectional and nonlinear wave group shoaling. *Ocean Dyn.* **71** (11), 1105–1112.

LAWRENCE, C., TRULSEN, K. & GRAMSTAD, O. 2021 Statistical properties of wave kinematics in long-crested irregular waves propagating over non-uniform bathymetry. *Phys. Fluids* **33** (4), 046601.

LAWRENCE, C., TRULSEN, K. & GRAMSTAD, O. 2022 Extreme wave statistics of surface elevation and velocity field of gravity waves over a two-dimensional bathymetry. *J. Fluid Mech.* **939**, A41.

LI, Y., DRAYCOTT, S., ZHENG, Y., LIN, Z., ADCOCK, T.A.A. & BREMER, T.S. 2021 Why rogue waves occur atop abrupt depth transitions. *J. Fluid Mech.* **919**, R5.

LIU, P.L.F. & DINGEMANS, M.W. 1989 Derivation of the third-order evolution equations for weakly nonlinear water waves propagating over uneven bottoms. *Wave Motion* **11** (1), 41–64.

LONGUET-HIGGINS, M. 1963 The effect of nonlinearities on statistical distributions in the theory of sea waves. *J. Fluid Mech.* **17** (3), 459–480.

LYU, Z., MORI, N. & KASHIMA, H. 2021 Freak wave in high-order weakly nonlinear wave evolution with bottom topography change. *Coast. Engng* **167**, 103918.

MA, Y., DONG, G. & MA, X. 2014 Experimental study of statistics of random waves propagating over a bar. *Coast. Engng Proc.* **34**, 30.

MAJDA, A.J., MOORE, M.N.J. & QI, D. 2019 Statistical dynamical model to predict extreme events and anomalous features in shallow water waves with abrupt depth change. *Proc. Natl Acad. Sci.* **116** (10), 3982–3987.

MCLEAN, J.W., MA, Y.C., MARTIN, D.U., SAFFMAN, P.G. & YUEN, H.C. 1981 Three-dimensional instability of finite-amplitude water waves. *Phys. Rev. Lett.* **46** (13), 817–820.

MEI, C.C. & BENMOUSSA, C. 1984 Long waves induced by short-wave groups over an uneven bottom. *J. Fluid Mech.* **139**, 219–235.

MENDES, S., SCOTTI, A., BRUNETTI, M. & KASPARIAN, J. 2022 Non-homogeneous analysis of rogue wave probability evolution over a shoal. *J. Fluid Mech.* **939**, A25.

MORI, N. & JANSSEN, P.A.E.M. 2006 On kurtosis and occurrence probability of freak waves. *J. Phys. Oceanogr.* **36** (7), 1471–1483.

MORI, N., ONORATO, M. & JANSSEN, P.A.E.M. 2011 On the estimation of the kurtosis in directional sea states for freak wave forecasting. *J. Phys. Oceanogr.* **41** (8), 1484–1497.

MORI, N., ONORATO, M., JANSSEN, P.A.E.M., OSBORNE, A.R. & SERIO, M. 2007 On the extreme statistics of long-crested deep-water waves: theory and experiments. *J. Geophys. Res: Oceans* **112**, C09011.

NÆSS, A. 1985 The joint crossing frequency of stochastic processes and its application to wave theory. *Appl. Ocean Res.* **7** (1), 35–50.

NIKOLKINA, I. & DIDENKULOVA, I. 2011 Rogue waves in 2006–2010. *Nat. Hazards Earth Syst. Sci.* **11** (11), 2913–2924.

ONORATO, M. *et al*. 2009*a* Statistical properties of mechanically generated surface gravity waves: a laboratory experiment in a three-dimensional wave basin. *J. Fluid Mech.* **627**, 235–257.

ONORATO, M. *et al*. 2009*b* Statistical properties of directional ocean waves: the role of the modulational instability in the formation of extreme events. *Phys. Rev. Lett.* **102** (11), 114502.

PEREGRINE, D.H. 1983 Water waves, nonlinear Schrödinger equations and their solutions. *ANZIAM J.* **25** (1), 16–43.

SERGEEVA, A., PELINOVSKY, E. & TALIPOVA, T. 2011 Nonlinear random wave field in shallow water: variable Korteweg-de Vries framework. *Nat. Hazards Earth Syst. Sci.* **11** (2), 323–330.

TRULSEN, K., RAUSTØL, A., JORDE, S. & RYE, L. 2020 Extreme wave statistics of long-crested irregular waves over a shoal. *J. Fluid Mech.* **882**, R2.

TRULSEN, K., ZENG, H. & GRAMSTAD, O. 2012 Laboratory evidence of freak waves provoked by non-uniform bathymetry. *Phys. Fluids* **24** (9), 097101.

TURPIN, F.-M., BENMOUSSA, C. & MEI, C.C. 1983 Effects of slowly varying depth and current on the evolution of a Stokes wavepacket. *J. Fluid Mech.* **132**, 1–23.

VIOTTI, C. & DIAS, F. 2014 Extreme waves induced by strong depth transitions: fully nonlinear results. *Phys. Fluids* **26** (5), 051705.

WASEDA, T. 2006 Impact of directionality on the extreme wave occurrence in a discrete random wave system. In *Proceedings of 9th International Workshop on Wave Hindcasting and Forecasting*, Victoria, Canada, p. 8. Environment Canada.

WASEDA, T., KINOSHITA, T. & TAMURA, H. 2009 Evolution of a random directional wave and freak wave occurrence. *J. Phys. Oceanogr.* **39**, 621–639.

YUEN, H. & LAKE, B. 1982 Nonlinear dynamics of deep-water gravity waves. *Adv. Appl. Mech.* **22**, 67–229.

ZAKHAROV, V.E. 1968 Stability of periodic waves of finite amplitude on the surface of a deep fluid. *J. Appl. Mech. Tech. Phys.* **9** (2), 190–194.

ZENG, H. & TRULSEN, K. 2012 Evolution of skewness and kurtosis of weakly nonlinear unidirectional waves over a sloping bottom. *Nat. Hazards Earth Syst. Sci.* **12** (3), 631.

ZHANG, J., MICHEL BENOIT, M., KIMMOUN, O., CHABCHOUB, A. & HSU, H.-C. 2019 Statistics of extreme waves in coastal waters: large scale experiments and advanced numerical simulations. *Fluids* **4** (2), 99.

ZHENG, Y., LIN, Z., LI, Y., ADCOCK, T.A.A., LI, Y. & BREMER, T.S. 2020 Fully nonlinear simulations of unidirectional extreme waves provoked by strong depth transitions: the effect of slope. *Phys. Rev. Fluids* **5** (6), 064804.